Simulating Magnetic Circular Dichroism Spectra

with Real-Time Time-Dependent Density

Functional Theory in Gauge Including Atomic

Orbitals

Shichao Sun, Ryan Beck, David Williams-Young, and Xiaosong Li*

Department of Chemistry, University of Washington, Seattle, WA, 98195

E-mail: xsli@uw.edu

Abstract

Magnetic circular dichroism (MCD) spectra are able to provide insights to the geo-

metric, electronic, and magnetic properties of chemical systems. However, they can be

challenging to understand and simulate given the need to simultaneously treat both the

finite magnetic and optical fields. Thus, efficient simulations are desired to understand

the spectra and resolve the molecular electronic states. Real-time dynamics are used

widely in the simulation of electronic spectroscopies such as absorption as well as elec-

tronic circular dichroism, but simulating MCD with real-time dynamics is technically

and theoretically challenging. In this work, we introduce a real-time dynamics based ab

initio method with a non-perturbative treatment of a static magnetic field with London

orbitals for simulating the MCD spectra of closed-shell systems. Effects of a magnetic

field are included variationally in the spin-free non-relativistic Hamiltonian. Real-time

time dependent density functional theory dynamics are then performed, from which

we compute the response function in the presence of the external magnetic field, giving

1

the MCD spectrum. The method developed in this paper is applied to simulate the MCD spectra for pyrimidine, pyrazine, and 1,4-naphthoquinone. Results are discussed and compared to experiment.

1 Introduction

In magnetic circular dichroism (MCD) experiments, the breaking of degeneracies due to the application of a magnetic field, which couples the (spin and/or orbital) angular momentum to the field, giving rise to additional spectroscopic features that are otherwise inaccessible at zero field. There have been many successful developments to compute MCD spectra with response theory including single residue of the quadratic response function,² the complex polarization propagator method, ^{3–5} and magnetically perturbed time-dependent density functional theory (TDDFT). 6-8 Configuration interaction (CI) base techniques include truncated CI with a sum-over-states expression and a perturbative treatment of the magnetic field and spin-orbit coupling, ^{9,10} as well as a multi-configurational self-consistent-field (MC-SCF) with quasi-degenerate perturbation theory to include Zeeman effects with spin-couplings. 11-13 The technique of using London orbitals at zero magnetic field has been applied in the perturbative calculation of MCD at the level of EOM-CC, TDHF, and TDDFT, mitigating the gauge-origin dependence of finite atom-centered basis sets. 14-17 Recently, a new class of ab initio computational MCD methods using a variational treatment of the magnetic field has been developed within the linear response complex time-dependent Hartree-Fock (\mathbb{C} -TDHF) framework. 18

Compared to response theory based methods, real-time time-dependent theory has many unique advantages. Real-time approaches can resolve a broad spectra in a single short time simulation. This is particularly useful for systems with high density of states. For DFT based methods, real-time dynamics also avoid the implementation of functional second derivatives. We refer readers to Ref. 19 for a recent review on real-time electronic structure theory. For absorption spectra and electronic circular dichroism, ^{20,21} real-time approaches only need

to treat the perturbing electric field. The calculation of MCD spectra, however, requires the inclusion of both static magnetic and perturbing electric fields. Real-time electronic dynamics using a real-space local density approximation (LDA) have been applied to simulate effective $\mathscr A$ and $\mathscr B$ terms of MCD spectra. ²²

Within the density functional theory framework, advanced functional formalisms have been developed to describe molecules in the presence of a magnetic field. The inclusion of a magnetic field effect has been represented either by the functional dependence of current density in current-density-functional theory (CDFT)^{23–28} or the functional dependence of the magnetic field in magnetic-field density functional theory (BDFT), ^{29,30} where both of these methods can be mathematically shown as equivalent. ³¹ When compared to full-configuration interaction, it has been observed that the exchange-correlation functional does not depend strongly on the magnetic field. ²⁹

In this paper, we introduce a real-time TDDFT approach using the generalized gradient approximation (GGA) of the magnetic-field density functional theory in an atomic orbital basis. In the time-dependent variational approach, the treatment of the magnetic perturbation is included non-perturbatively. Effects of a static, uniform magnetic field are included variationally with London orbitals, ^{18,32–40} which provide the most satisfactory solution to correct for the gauge-origin problem when an incomplete Gaussian-type basis is used. ^{41–48}

2 Methodology

2.1 Computing MCD Spectrum with Real-Time Electronic Structure Methods

MCD spectrum measures the response of a molecular system perturbed by a static magnetic field and probed by left and right circularly polarized light. This type of measurement can be described by a time-dependent Hamiltonian which consists of a time-independent and a time-dependent component, $H = H_0 + V_t$.

The magnetic field perturbations can be described by the time-independent Hamiltonian, $H_0 = h_0 + W$, where W is the two-electron interaction, and h_0 is the one-electron Hamiltonian. ^{18,40}

$$h_0 = -\frac{1}{2}\mathbf{\nabla}^2 + \frac{1}{2}(-i\mathbf{r} \times \nabla) \cdot \mathbf{B} + \frac{1}{8}(\mathbf{B} \times \mathbf{r})^2 + \sum_A \frac{Z_A}{|\mathbf{r} - \mathbf{R}_A|}$$
(1)

The second term in Eq. (1) includes orbital Zeeman contributions, and the third term describes diamagnetism of a molecular system.

Using the electric-dipole approximation in the length gauge, $V_t = -\mathbf{r} \cdot \mathbf{E}_W$, for the interaction between the system and the probing optical field, the MCD spectra (in molar ellipticity with the conventional unit of Degree(mol/L)⁻¹m⁻¹Gauss⁻¹) can be computed using the following expression⁷

$$[\theta]_M = \Gamma \sum_J R_J \omega f(\omega - \omega_{0J}^{\gamma}) \tag{2}$$

where the rotatory strength R_J is defined as:

$$R_{J} = -\frac{1}{3} \frac{\sum_{\alpha\beta\gamma} \varepsilon_{\alpha\beta\gamma} \operatorname{Im}(\langle 0 | \mu_{\alpha} | J \rangle^{\gamma} \langle J | \mu_{\beta} | 0 \rangle^{\gamma})}{\mu_{B} |\mathbf{B}|}$$
(3)

 $\langle 0 | \mu_{\alpha} | J \rangle$ is the transition dipole and ω_{0J}^{γ} is the excitation energy from ground state to the excited state J in the presence of a static magnetic field. $f(\omega - \omega_{0J}^{\gamma})$ is the band shape function, which for fixed molecular structures we assume infinite excited state lifetime, thus $f(\omega - \omega_{0J}^{\gamma})$ can be written as a delta function, $\delta(\omega - \omega_{0J}^{\gamma})$. $\epsilon_{\alpha\beta\gamma}$ is Levi-Civita symbol $(\epsilon_{xyz} = \epsilon_{yzx} = \epsilon_{zxy} = 1, \epsilon_{yxz} = \epsilon_{xzy} = \epsilon_{zyx} = -1,$ otherwise 0). Γ is a collection of physical constants. 49 R_J , ω , and f are in atomic units. We use superscript γ to explicitly denote the direction of the applied magnetic field. For detailed derivation of this expression, we refer readers to Reference 18.

2.1.1 Relating MCD Spectrum to Response Function Formalism

Thus, in order to compute MCD spectra using Eq. (2), one needs to extract the imaginary component of the quantity $\langle 0 | \mu_{\alpha} | J \rangle^{\gamma} \langle J | \mu_{\beta} | 0 \rangle^{\gamma}$ from RT-TDDFT electronic dynamics. However, this is not a quantity that can be easily obtained from direct analyses of time-dependent observables, e.g., Fourier transformation of electric dipoles. In this work, we propose a response function based technique that can be used to resolve MCD spectra from real-time electronic structure simulations. In the following, we will present derivations that transform Eq. (2) into a response function formalism of the time-dependent signals.

We start by using the following expression,

$$\sum_{J} \operatorname{Im}(A_{0J}^{\alpha\beta,\gamma}) \delta(\omega - \omega_{0J}^{\gamma}) \approx \sum_{J} \left[\operatorname{Im}(A_{0J}^{\alpha\beta,\gamma}) \delta(\omega - \omega_{0J}^{\gamma}) - \operatorname{Im}(A_{0J}^{\beta\alpha,\gamma}) \delta(\omega + \omega_{0J}^{\gamma}) \right]$$
(4)

where

$$A_{0J}^{\alpha\beta,\gamma} = \langle 0 | \mu_{\alpha} | J \rangle^{\gamma} \langle J | \mu_{\beta} | 0 \rangle^{\gamma} = (A_{0J}^{\beta\alpha,\gamma})^*$$
 (5)

The δ function in Eq. (4) can be defined as the following limit,⁵⁰

$$\delta(\omega - \omega_{0J}^{\gamma}) = \frac{1}{\pi} \lim_{\eta \to 0^+} \frac{\eta}{(\omega - \omega_{0J}^{\gamma})^2 + \eta^2}$$
(6)

Using this relationship, Eq. (4) can be written as,

$$\sum_{J} \operatorname{Im}(A_{0J}^{\alpha\beta,\gamma}) \delta(\omega - \omega_{0J}^{\gamma})
\approx \frac{1}{\pi} \sum_{J} \lim_{\eta \to 0^{+}} \left[\frac{\operatorname{Im}(A_{0J}^{\alpha\beta,\gamma}) \eta}{(\omega - \omega_{0J}^{\gamma})^{2} + \eta^{2}} - \frac{\operatorname{Im}(A_{0J}^{\beta\alpha,\gamma}) \eta}{(\omega + \omega_{0J}^{\gamma})^{2} + \eta^{2}} \right]
= \frac{1}{\pi} \sum_{J} \lim_{\eta \to 0^{+}} \left[\frac{\operatorname{Im}(A_{0J}^{\alpha\beta,\gamma}) \eta}{(\omega - \omega_{0J}^{\gamma} + i\eta)(\omega - \omega_{0J}^{\gamma} - i\eta)} - \frac{\operatorname{Im}(A_{0J}^{\beta\alpha,\gamma}) \eta}{(\omega + \omega_{0J}^{\gamma} + i\eta)(\omega + \omega_{0J}^{\gamma} - i\eta)} \right]$$
(7)

Recognizing that $\text{Re}[A_{0J}^{\alpha\beta,\gamma}-(A_{0J}^{\alpha\beta,\gamma})^*]=0$ and $\text{Im}[A_{0J}^{\alpha\beta,\gamma}-(A_{0J}^{\alpha\beta,\gamma})^*]=2\text{Im}(A_{0J}^{\alpha\beta,\gamma})$, we can

rewrite Eq. (7) and factor out $\omega - \omega_{0J}^{\gamma} - i\eta$ and $\omega + \omega_{0J}^{\gamma} - i\eta$ in the denominators,

$$\frac{1}{2\pi} \sum_{J} \lim_{\eta \to 0^{+}} \left(\frac{\frac{\operatorname{Re}[A_{0J}^{\alpha\beta,\gamma} - (A_{0J}^{\alpha\beta,\gamma})^{*}](\omega - \omega_{0J}^{\gamma}) + \operatorname{Im}[A_{0J}^{\alpha\beta,\gamma} - (A_{0J}^{\alpha\beta,\gamma})^{*}]\eta}{(\omega - \omega_{0J}^{\gamma} + i\eta)(\omega - \omega_{0J}^{\gamma} - i\eta)} \right) \\
= \frac{1}{2\pi} \sum_{J} \lim_{\eta \to 0^{+}} \operatorname{Re} \left[\frac{[A_{0J}^{\alpha\beta,\gamma} - (A_{0J}^{\alpha\beta,\gamma})^{*}](\omega + \omega_{0J}^{\gamma}) + \operatorname{Im}[A_{0J}^{\alpha\beta,\gamma} - (A_{0J}^{\beta\alpha,\gamma})^{*}]\eta}{(\omega + \omega_{0J}^{\gamma} + i\eta)(\omega + \omega_{0J}^{\gamma} - i\eta)} - \frac{[A_{0J}^{\beta\alpha,\gamma} - (A_{0J}^{\beta\alpha,\gamma})^{*}](\omega + \omega_{0J}^{\gamma} - i\eta)}{(\omega + \omega_{0J}^{\gamma} - i\eta)} \right] \\
= \frac{1}{2\pi} \sum_{J} \lim_{\eta \to 0^{+}} \operatorname{Re} \left[\frac{A_{0J}^{\alpha\beta,\gamma} - (A_{0J}^{\alpha\beta,\gamma})^{*}}{(\omega - \omega_{0J}^{\gamma} + i\eta)(\omega - \omega_{0J}^{\gamma} - i\eta)} - \frac{A_{0J}^{\beta\alpha,\gamma} - (A_{0J}^{\beta\alpha,\gamma})^{*}}{(\omega + \omega_{0J}^{\gamma} + i\eta)(\omega + \omega_{0J}^{\gamma} - i\eta)} \right]$$

$$(8)$$

Using the definition of the response function $\langle \mu_{\alpha}; \mu_{\beta} \rangle_{\omega}^{\gamma}$, 51,52

$$\langle\!\langle \mu_{\alpha}; \mu_{\beta} \rangle\!\rangle_{\omega}^{\gamma} = \lim_{\eta \to 0^{+}} \frac{\langle 0 | \mu_{\alpha} | J \rangle^{\gamma} \langle J | \mu_{\beta} | 0 \rangle^{\gamma}}{\omega - \omega_{0J} + i\eta} - \frac{\langle 0 | \mu_{\beta} | J \rangle^{\gamma} \langle J | \mu_{\alpha} | 0 \rangle^{\gamma}}{\omega + \omega_{0J} + i\eta}$$
(9)

it is easy to see that Eq. (4) in the form of Eq. (8) can be simplified to

$$\sum_{J} \operatorname{Im}(A_{0J}^{\alpha\beta,\gamma}) \delta(\omega - \omega_{0J}^{\gamma}) \approx \frac{1}{2\pi} \sum_{J} \operatorname{Re}(\langle\langle \mu_{\alpha}; \mu_{\beta} \rangle\rangle_{\omega}^{r} - \langle\langle \mu_{\beta}; \mu_{\alpha} \rangle\rangle_{\omega}^{r})$$
(10)

The final working equation for calculating MCD spectra becomes,

$$[\theta]_{M} = -\frac{\Gamma}{3\mu_{B}|\mathbf{B}|} \sum_{\alpha\beta\gamma} \omega \varepsilon_{\alpha\beta\gamma} \operatorname{Im}(\langle 0 | \mu_{\alpha} | n \rangle^{\gamma} \langle n | \mu_{\beta} | 0 \rangle^{\gamma}) \delta(\omega - \omega_{0J}^{\gamma})$$

$$= -\frac{\Gamma}{6\pi\mu_{B}|\mathbf{B}|} \sum_{\alpha\beta\gamma} \omega \varepsilon_{\alpha\beta\gamma} \operatorname{Re}(\langle \mu_{\alpha}; \mu_{\beta} \rangle)_{\omega}^{\gamma} - \langle \mu_{\beta}; \mu_{\alpha} \rangle_{\omega}^{\gamma})$$
(11)

Calculating MCD spectra using the first expression in Eq. (11) requires the computation of the transition dipole moments and excitation energies in the presence of an external magnetic field. These quantities can be obtained using the linear response formalism of the TDHF/TDDFT equation. ¹⁸ Alternatively, MCD spectra can be evaluated using the second expression in Eq. (11) which works with real-time time-dependent electronic structure methods.

2.1.2 Relating Time-Dependent Signals to Response Function Formalism

In this section, we will derive the relationship between the response function formalism in Eq. (11) and time-dependent signals obtained from real-time simulations. We will assume a variational treatment of the static magnetic field applied in the $\gamma \in x, y, z$ direction and that all time-dependent observables are collected in the presence of the magnetic field.

With an electrical δ -kick of intensity κ applied at t=0 in direction $\beta \in x, y, z$, the perturbation Hamiltonian of the electric field can be expanded in the frequency domain as

$$\hat{V}_t = \delta(t)\hat{\mu}_{\beta}^{\gamma}\kappa_{\beta} = \frac{\hat{\mu}_{\beta}^{\gamma}\kappa_{\beta}}{2\pi} \int_{-\infty}^{\infty} e^{-i\omega t} d\omega$$
 (12)

where all the frequencies have the same amplitude. Such an electric field perturbation will lead to the time-evolution of the dipole moment of a molecular system.

The time-evolution of the α -component of the dipole moment, μ_{α} , can be expressed as ⁵¹

$$\mu_{\alpha}^{\gamma}(t) - \mu_{\alpha}^{\gamma}(0) = -\int_{-\infty}^{t} i\langle 0|[\hat{\mu}_{\alpha}, e^{i\hat{H}_{0}(t'-t)}\hat{V}_{t'} e^{-i\hat{H}_{0}(t'-t)}]|0\rangle^{\gamma} dt'$$
(13)

Substituting Eq. (12) into the Eq. (13) followed by a time-frequency transformation, we have

$$\mu_{\alpha}^{\gamma}(\omega) = \int_{-\infty}^{\infty} (\mu_{\alpha}^{\gamma}(t) - \mu_{\alpha}^{\gamma}(0))e^{i\omega t}dt$$

$$= -\frac{\kappa_{\beta}}{2\pi} \int_{-\infty}^{\infty} e^{i\omega t}dt \int_{-\infty}^{\infty} e^{-i\omega' t}d\omega' \int_{-\infty}^{t} i\langle 0|[\hat{\mu}_{\alpha}, e^{i\hat{H}_{0}(t'-t)}\hat{\mu}_{\beta} e^{-i\hat{H}_{0}(t'-t)}]|0\rangle^{\gamma} dt' \qquad (14)$$

One can show that Eq. (14) can be equivalently written in a response function form, ^{51,52}

$$\mu_{\alpha}^{\gamma}(\omega) = \kappa_{\beta} \langle \langle \mu_{\alpha}; \mu_{\beta} \rangle \rangle_{\omega}^{\gamma} \tag{15}$$

where the response function is defined in Eq. (9). For detailed derivation, we refer readers to Reference 51.

Using Eq. (15) in Eq. (11), we can write the final expression for computing the MCD molar ellipticity in Degree(mol/L)⁻¹m⁻¹Gauss⁻¹ using quantities in atomic units calculated from real-time electronic dynamics:

$$[\theta]_M = -0.0014802 \times \frac{1}{6\pi |\mathbf{B}|} \sum_{\alpha\beta\gamma} \omega \,\varepsilon_{\alpha\beta\gamma} \operatorname{Re}\left(\frac{\mu_{\alpha}^{\gamma}(\omega)}{\kappa^{\beta}} - \frac{\mu_{\beta}^{\gamma}(\omega)}{\kappa^{\alpha}}\right) \tag{16}$$

where $\mu_{\alpha}^{\gamma}(\omega)$, ω , $|\mathbf{B}|$, κ^{β} are in atomic units.

Note that the working equation Eq. (16) is similar to that in Reference 22 which was derived via the perturbation of wave function. The derivation presented here builds a connection between the real-time signal and the response function formalism. This approach is also generally applicable to other types of spectra. Observables computed using the linear response function with the non-perturbative treatment of magnetic field derived herein are similar to those calculated using the quadratic response function² or the gradient of linear response. ^{6–8}

Since the non-perturbative treatment of magnetic field can account for the splitting of excited states and perturbation of transition dipole at the orbital level, the response theory based formalism presented here is able to treat the effects equivalent to $\mathscr A$ and $\mathscr B$ terms. However, the simulation of $\mathscr C$ term effect of open-shell system requires the inclusion of spin-orbit coupling, which cannot be simulated directly using the non-relativistic formalism.

2.2 Density-Functional Theory with Complex-Valued Orbitals

The molecular orbitals are expanded in a basis of complex-valued London orbitals.³²

$$\phi_j(\mathbf{r}) = \sum_{\mu} C_{\mu j} \tilde{\chi}_{\mu}(\mathbf{r}, \mathbf{k}_A) \tag{17}$$

$$\tilde{\chi}_{\mu}(\mathbf{r}, \mathbf{k}_{A}) = \chi_{\mu}(\mathbf{r} - \mathbf{R}_{A})e^{i\mathbf{k}_{A}\cdot(\mathbf{r} - \mathbf{R}_{A})}$$
(18)

where $\{\chi_{\mu}(\mathbf{r} - \mathbf{R}_A)\}$ are real atomic orbital (AO) basis functions centered at \mathbf{R}_A . The exponential form of the London orbital phase factor defines the local gauge origin at each nuclear center in the presence of magnetic field with a plane wave vector described by $\mathbf{k}_A = \frac{\mathbf{R}_A \times \mathbf{B}}{2}$, where \mathbf{B} is the external magnetic field.

In the presence of an external magnetic field, the Kohn-Sham matrix in the London orbital basis for a closed-shell system is defined as: ²⁸

$$\mathbf{F}' = \mathbf{T} + \mathbf{V} + \mathbf{J}[\mathbf{P}'] + \mathbf{V}^{\mathrm{xc}}[\mathbf{P}'] - \frac{1}{2}c_{\mathbf{x}}\mathbf{K}[\mathbf{P}'] - \frac{i}{2}\mathbf{L} \cdot \mathbf{B}$$

$$+ \frac{1}{8} \left\{ (B_y^2 + B_z^2)\mathbf{q}_{xx} + (B_x^2 + B_z^2)\mathbf{q}_{yy} + (B_x^2 + B_y^2)\mathbf{q}_{zz} \right.$$

$$- 2B_x B_y \mathbf{q}_{xy} - 2B_y B_z \mathbf{q}_{yz} - 2B_x B_z \mathbf{q}_{xz} \right\}$$

$$(19)$$

where $\mathbf{L}_{\mu\nu} = \langle \tilde{\chi}_{\mu} | \mathbf{r} \times \boldsymbol{\nabla} | \tilde{\chi}_{\nu} \rangle$ and $\langle \mathbf{q}_{nm} \rangle_{\mu\nu} = (\tilde{\chi}_{\mu} | \hat{r}_{n} \hat{r}_{m} | \tilde{\chi}_{\nu} \rangle$ are the orbital-angular momentum and electric quadrupole integrals, respectively. We also use a primed notation for the magnetic field perturbed Kohn-Sham (\mathbf{F}') and density (\mathbf{P}') matrices. Equation (19) corresponds to a pure density functional when $c_{\mathbf{x}} = 0$.

The magnetic-field density functional theory formalism^{29,30} is used in this implementation, where the functional does not explicitly depend on the magnetic field. Since the magnetic field perturbs the electron density and its derivatives, the density functional will implicitly depend on the magnetic field.

The Coulomb (**J**) and exchange (**K**) matrix elements are defined as:

$$J_{\mu\nu}[\mathbf{P}'] = \sum_{\lambda\kappa} (\tilde{\chi}_{\mu}\tilde{\chi}_{\nu}|\tilde{\chi}_{\kappa}\tilde{\chi}_{\lambda})P'_{\lambda\kappa}$$
 (20)

$$K_{\mu\nu}[\mathbf{P'}] = \sum_{\lambda\kappa} (\tilde{\chi}_{\mu}\tilde{\chi}_{\lambda}|\tilde{\chi}_{\kappa}\tilde{\chi}_{\nu})P'_{\lambda\kappa}$$
 (21)

The recursive relationships for evaluating one- and two-electron integrals using complex valued London orbitals have been presented in Ref. 53.

Using London atomic orbitals in Kohn-Sham DFT also implies that the evaluation of

matrix elements of \mathbf{V}^{xc} requires a careful scrutiny because the density matrix and atomic orbitals are complex-valued. For GGA, the following quantities need to be evaluated on a numerical grid in order to compute the matrix element of $V_{\mu\nu}^{\text{xc}}$

$$V_{\mu\nu}^{\text{xc}} = \frac{\partial E^{\text{xc}}}{\partial P_{\nu\mu}}$$

$$= \sum_{i} w_{i} \left[\frac{\partial f^{\text{xc}}}{\partial \rho(\mathbf{r})} \tilde{\chi}_{\mu}^{*}(\mathbf{r}) \tilde{\chi}_{\nu}(\mathbf{r}) \right]_{\mathbf{r} = \mathbf{r}_{i}} + \sum_{i} w_{i} \left[\frac{\partial f^{\text{xc}}}{\partial \nabla \rho(\mathbf{r})} (\nabla \tilde{\chi}_{\mu}^{*}(\mathbf{r}) \tilde{\chi}_{\nu}(\mathbf{r}) + \tilde{\chi}_{\mu}^{*}(\mathbf{r}) \nabla \tilde{\chi}_{\nu}(\mathbf{r})) \right]_{\mathbf{r} = \mathbf{r}_{i}}$$
(22)

where i runs over all the grid points. $f^{\rm xc}$ defines a density functional that depends on density variables. The expressions for evaluating $\frac{\partial f^{\rm xc}}{\partial \rho}$ and $\frac{\partial f^{\rm xc}}{\partial \nabla \rho}$ are usually obtained through a chain rule using auxiliary density variables (see Refs. 53,54 for implementation details for both spin collinear and non-collinear cases.). $\{w_i\}$ are weights of the integration grid points based on the Becke multi-center numerical integration scheme. S5,56 Note that because London orbitals are complex valued, the \mathbf{V}^{xc} becomes a complex-valued quantity, even though $\frac{\partial f^{\rm xc}}{\partial \rho(\mathbf{r})}$, and $\frac{\partial f^{\rm xc}}{\partial \nabla \rho(\mathbf{r})}$ are real-valued quantities in the KS formalism and real-time dynamics.

In the evaluation of density and basis set gradients, the derivative of primitive London atomic orbitals with respect to electronic coordinate \mathbf{r}_j is needed. The following expression is derived and used in this work,

$$\frac{\partial}{\partial r_{j}}\tilde{g}_{\mu}(\mathbf{r} - \mathbf{R}_{A}; \mathbf{k}_{A}; \mathbf{a}; \zeta_{\alpha})$$

$$= -2\zeta_{\alpha}\tilde{g}_{\mu}(\mathbf{r} - \mathbf{R}_{A}; \mathbf{k}_{A}; \mathbf{a} + \mathbf{1}_{j}; \zeta_{\alpha}) + a_{j}\tilde{g}_{\mu}(\mathbf{r} - \mathbf{R}_{A}; \mathbf{k}_{A}; \mathbf{a} - \mathbf{1}_{j}; \zeta_{\alpha}) + i(k_{A})_{j}\tilde{g}_{\mu}(\mathbf{r} - \mathbf{R}_{A}; \mathbf{k}_{A}; \mathbf{a}; \zeta_{\alpha})$$
(23)

where g is the primitive London atomic orbitals centered at \mathbf{R}_A with orbital angular momentum \mathbf{a} and Gaussian exponent ζ .

2.3 Equation-of-Motion of Real-Time TDDFT

The evolvement of the system is by a time-integration of the Liouville-von Neumann equation:

$$i\frac{\partial \mathbf{P}}{\partial t} = [\mathbf{F}, \mathbf{P}] \tag{24}$$

with the modified midpoint and unitary transformation (MMUT) approach. ^{19,57–60} See 19 for a recent review on RT-TDDFT.

3 Computational Detail

All molecular geometries were optimized 61 in the absence of a magnetic field using the GAUSSIAN16 computational chemistry software package 62 using the B3LYP $^{63-65}$ functional and the 6-31G(d) basis. 66,67

RT-TDDFT calculations in a magnetic filed with a GIAO basis were carried out with the CHRONUS QUANTUM open source package⁶⁸ using the B3LYP⁶³⁻⁶⁵ functional and the London-6-31G(d) basis. ^{66,67} The magnetic field strength is 2.238×10^{-5} a.u. (~5.26 T), comparable to that used in experiments. ^{69,70} At t < 0, the ground state SCF was converged with a magnetic field applied in direction γ . The external magnetic field is applied throughout the RT-TDDFT dynamics. At t = 0, an electrical δ -kick is applied in the direction β . After the pulse, the system evolves according to Eq. (24). At each timestep, the expectation value of electric dipole $\mu(t)$ is evaluated. In order to obtain a spectral broadening, a damping factor, Γ , in the Fourier transformation is used:

$$\mu_{\alpha}^{\gamma}(\omega) = \int_{-\infty}^{\infty} (\mu_{\alpha}^{\gamma}(t) - \mu_{\alpha}^{\gamma}(0)) \exp\left(-\frac{t}{\Gamma}\right) e^{i\omega t} dt$$
 (25)

The value of Γ is determined in order to reproduce the experimental linewidth. Six separate dynamics for each test molecule are carried out with the external magnetic fields applied in the x, y, and z directions and a pulsed electric field in two directions orthogonal to the

magnetic field. The simulation stepsize is 0.05 a.u. (~ 0.0012 fs). The simulation time is 100 fs for pyrimidine, pyrazine and 1,4-naphthoquinone and 500 fs for sodium anion. The electric field strength is 10^{-5} a.u.

4 Benchmark and Discussion

4.1 Sodium Anion

Figure 1 compares the MCD spectra of sodium anion in a 5.0×10^{-5} a.u. (~ 11.75 T) magnetic field, computed with the real-time TDHF and the linear response TDHF formalisms, respectively. ¹⁸ The MCD spectra computed using these two different methods are indistinguishable. An external magnetic field introduces orbital Zeeman interactions that break the three-fold degeneracy of the p orbitals, giving rise to two peaks of opposite sign which leads to a derivative shape, shown in Fig. 1. This benchmark shows that the real-time and the linear response approaches produce equivalent MCD spectra at the weak field limit.

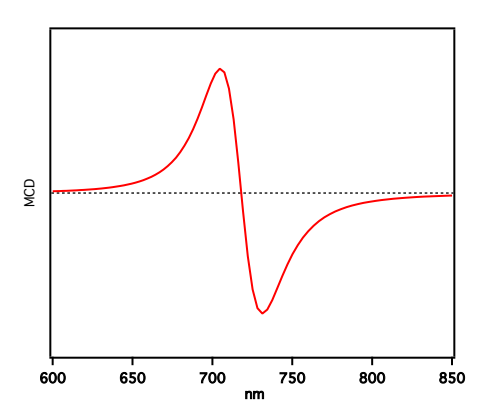


Figure 1. Simulated MCD spectra of Na⁻ $s \to p$ transitions in a 5×10^{-5} a.u. (~11.75 T) magnetic field. An arbitrary unit and spectral broadening with a damping factor of $\Gamma = 500$ a.u. are used.

4.2 Pyrimidine and Pyrazine

Pyrimidine and pyrazine are structural isomers of six-membered heterocyclic ring (Fig. 2). With UV/Vis absorption spectroscopy, these two isomers are not differentiable because they

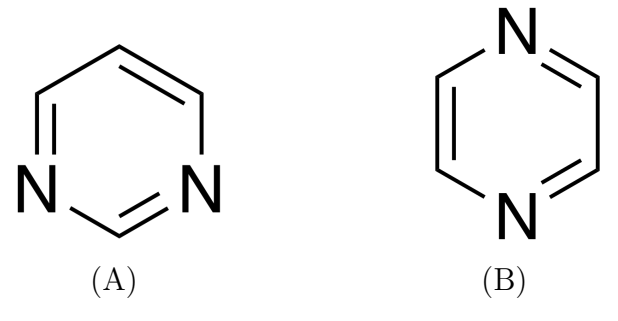


Figure 2. (A) Pyrimidine, (B) Pyrazine

have very similar linear absorption spectra. In this case, MCD can be a powerful experimental tool to analyze the photochemical properties of structural isomers due to the difference in their point group symmetry. In addition, since their $n \to \pi^*$ and $\pi \to \pi^*$ transitions give rise to alternating positive and negative MCD peaks, they are frequently used as benchmark systems for theoretical simulations. 7,14,15,17,69,70

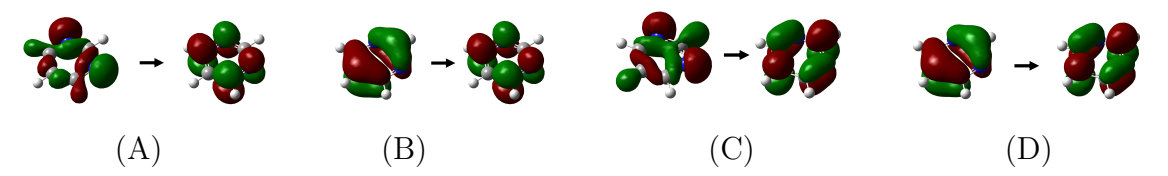


Figure 3. Main molecular orbital contributions to optical excitations in pyrimidine

In the C_{2v} point group, pyrimidine has several low-lying allowed optical transitions. The first peak at 3.5×10^4 cm⁻¹ is the $n \to \pi^*$ transition, giving rise to the the $1B_1$ excited state, with corresponding molecular orbitals shown in Fig. 3A. The next two excitations are associated with the $1B_2$ and $2B_1$ excited states, with the $\pi \to \pi^*$ (Fig. 3B) and $n \to \pi^*$ (Fig. 3C) characteristics, located at 4.7×10^4 cm⁻¹ and 4.9×10^4 cm⁻¹, respectively. The last, and strongest, excitation in this simulated spectral range is the $\pi \to \pi^*$ excitation (Fig. 3D) from the ground state to the $1A_1$ state.

The pyrazine molecule has the D_{2h} symmetry. The first peak at 3.1×10^4 cm⁻¹ corresponds to the excitation from the ground state to the B_{3u} state. This transition is dominated by the $n \to \pi^*$ transition, where the electron in the lone pair orbital of N atom is excited to π^*

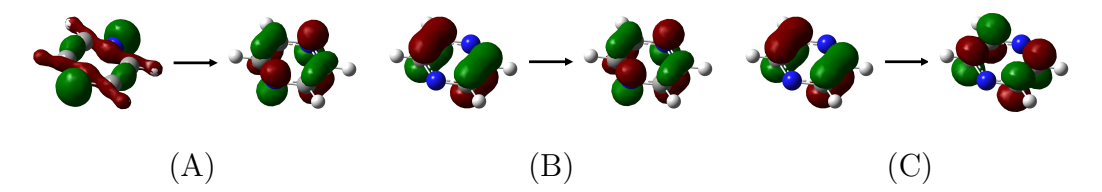


Figure 4. Main molecular orbital contributions to optical excitations in pyrazine.

orbital (Fig. 4A). The next two excitations in pyrazine both have the $\pi \to \pi^*$ character and give rise to the B_{2u} and B_{1u} states (Fig. 4B and Fig. 4C).

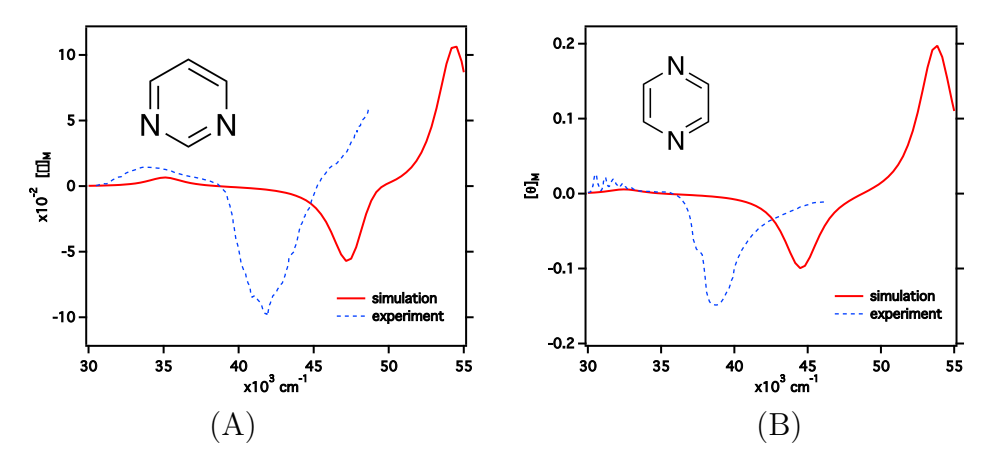


Figure 5. Simulated MCD spectra of pyrimidine (Fig. 5A) and pyrazine (Fig. 5B) in a 2.238×10^{-5} a.u. (~ 5.26 T) magnetic field, with a damping factor of 150 a.u. Experimental MCD spectra from Ref. 69 are also plotted in dashed blue curves.

The MCD spectra of pyrimidine and pyrazine computed using the RT-TDDFT method introduced in this paper are shown in Fig. 5, compared to experiments. ^{69,70} For these closed shell molecules, the excited states with singlet spins have no degeneracy. Therefore, the MCD signals is driven by the \mathscr{B} term, which is caused by the magnetic perturbation to the transition dipole. The estimated energies for these characteristic excitations (ω'_{0J}) from the real-time spectra are summarized in Tab. 1 and compared to absorption peaks (ω_{0J}) in the absence of the external magnetic field. The computed $n \to \pi^*$ transitions are in excellent agreement with experimental measurements. However, the $\pi \to \pi^*$ transitions in both molecules are blue-shifted by 0.6 eV, compared to experiments, although the computed signs and relative magnitudes of all transitions are in agreement with experiments.

Compared to the absorption spectra of linearly polarized light, although the presence of an external magnetic field gives rise to a different spectral shape it only slightly shifts the spectral positions. This comparison suggests that the disagreement with experiments is likely due to the choice of functional. These results, computed using the time-dependent variational method, are also consistent with calculations using the excited state gradients. ¹⁷ Perturbative calculations overestimate the magnitude of the 1B₂ state of pyrimidine and this work underestimated its intensity compared to the experiment.

Table 1. Excitation energies of pyrimidine and pyrazine molecules in a 2.238×10^{-5} a.u. (~ 5.26 T) magnetic field. ω'_{0J} is the estimated excitation energy from the real-time spectra. ω_{0J} is the excitation energy computed using the linear response formalism of the corresponding TDDFT in the absence of the external magnetic field.

Pyrimidine	$\omega_{0J}^{\prime}/\mathrm{cm}^{-1}$	$\omega_{0J}/\mathrm{cm}^{-1}$
$1B_1$	3.512×10^4	3.506×10^4
$1B_2$	4.732×10^4	4.734×10^4
$2B_1$	4.916×10^4	4.880×10^4
$1A_1$	5.452×10^4	5.440×10^4

Pyrazine	$\omega'_{0J}/\mathrm{cm}^{-1}$	$\omega_{0J}/\mathrm{cm}^{-1}$
B_{3u}	3.077×10^4	3.248×10^4
B_{2u}	4.448×10^4	4.454×10^4
B_{1u}	5.385×10^4	5.376×10^4

4.3 1,4-Naphthoquinone

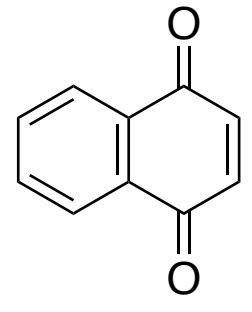


Figure 6. 1,4-naphthoguinone

The real-time approach is particularly convenient when simulating a broad spectral range with many excited states. Figure 7 plots the computed MCD spectrum of 1,4-naphthoquinone using the RT-TDDFT approach. Compared to the available experimental result ⁷¹ at the low energy range, the computed MCD spectrum are in good agreement with experiment. Figure 7B plots a broad energy range (0-30 eV) of the computed MCD spectrum. In contrast to solving for all excited states in a generalized eigenvalue problem, real-time approach can produce a broad band MCD spectrum with only three dynamic simulations.

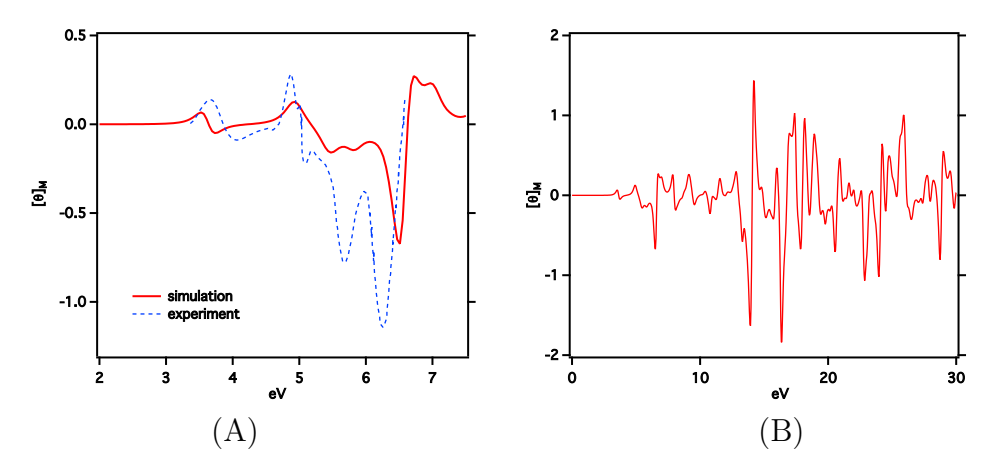


Figure 7. Simulated MCD spectrum of 1,4-naphthoquinone in a 2.238×10^{-5} a.u. (~ 5.26 T) magnetic field, with a damping factor of 150 a.u. Experimental MCD spectrum from Ref. 71 is also plotted in a dashed blue curve. Note that the experimental first ionization energy of 1,4-naphthoquinone is $\sim 9.4 \,\mathrm{eV}$. ⁷² Spectral features above the first ionization threshold correspond to excitations of deeper valence electrons.

5 Conclusion

In this paper, a real-time time-dependent density functional theory (RT-TDDFT) method, with a variational treatment of the static magnetic perturbation in London orbital basis, for simulating MCD spectra is developed and applied to several azaheterocycles. The MCD spectra can be obtained by the simulation of the linear response function. The Kohn-Sham formalism with finite magnetic field is extended to the time-dependent case at the level of hybrid functionals. Due to the use of London orbitals, the exchange-correlation energy and

potentials are evaluated with complex atomic orbitals.

RT-TDDFT simulations of pyrimidine and pyrazine predict correct signs of MCD absorption peaks, although excitation energies of the $\pi \to \pi^*$ transitions are blue-shifted compared to experiment. This work also highlights a unique advantage of the RT-TDDFT approach through the computation of a broad MCD spectrum of 1,4-Naphthoquinone using six dynamic simulations.

The scope of the simulation is limited to the effective \mathscr{A} and \mathscr{B} terms in MCD. Future directions include the development to enable the simulation of open-shell system MCD spectra and the \mathscr{C} term using the time-dependent variational approach.

Acknowledgement

The development of non-perturbative MCD methods is supported by the National Science Foundation (CHE-1856210). The development of the Chronus Quantum open source software package is supported by the National Science Foundation (OAC-1663636). Computations were facilitated through the use of advanced computational, storage, and networking infrastructure provided by the Hyak supercomputer system at the University of Washington, funded by the Student Technology Fee and the National Science Foundation (MRI-1624430).

References

- (1) Barron, L. D. Molecular Light Scattering and Optical Activity; Cambridge University Press, 2009.
- (2) Coriani, S.; Jørgensen, P.; Rizzo, A.; Ruud, K.; Olsen, J. Ab initio Determinations of Magnetic Circular Dichroism. Chem. Phys. Lett. 1999, 300, 61–68.
- (3) Solheim, H.; Ruud, K.; Coriani, S.; Norman, P. Complex Polarization Propagator Calculations of Magnetic Circular Dichroism Spectra. J. Chem. Phys. 2008, 128, 094103.
- (4) Krykunov, M.; Seth, M.; Ziegler, T.; Autschbach, J. Calculation of the Magnetic Circular Dichroism B Term from the Imaginary Part of the Verdet Constant Using Damped Time-Dependent Density Functional Theory. J. Chem. Phys. 2007, 127, 244102.
- (5) Solheim, H.; Ruud, K.; Coriani, S.; Norman, P. The A and B Terms of Magnetic Circular Dichroism Revisited. J. Phys. Chem. A 2008, 112, 9615–9618.
- (6) Seth, M.; Ziegler, T. Formulation of Magnetically Perturbed Time-Dependent Density Functional Theory. J. Chem. Phys. 2007, 127, 134108.
- (7) Seth, M.; Krykunov, M.; Ziegler, T.; Autschbach, J.; Banerjee, A. Application of Magnetically Perturbed Time-Dependent Density Functional Theory to Magnetic Circular Dichroism: Calculation of B Terms. J. Chem. Phys. 2008, 128, 144105.
- (8) Seth, M.; Krykunov, M.; Ziegler, T.; Autschbach, J. Application of Magnetically Perturbed Time-Dependent Density Functional Theory to Magnetic Circular Dichroism. II. Calculation of A Terms. J. Chem. Phys. 2008, 128, 234102.
- (9) Honda, Y.; Hada, M.; Ehara, M.; Nakatsuji, H.; Downing, J.; Michl, J. Relativistic Effects on Magnetic Circular Dichroism Studied by GUHF/SECI Method. Chem. Phys. Lett. 2002, 355, 219–225.

- (10) Honda, Y.; Hada, M.; Ehara, M.; Nakatsuji, H.; Michl, J. Theoretical Studies on Magnetic Circular Dichroism by the Finite Perturbation Method with Relativistic Corrections. J. Chem. Phys. 2005, 123, 164113.
- (11) Ganyushin, D.; Neese, F. First-Principles Calculations of Magnetic Circular Dichroism Spectra. J. Chem. Phys. 2008, 128, 114117.
- (12) Gendron, F.; Fleischauer, V. E.; Duignan, T. J.; Scott, B. L.; Löble, M. W.; Cary, S. K.; Kozimor, S. A.; Bolvin, H.; Neidig, M. L.; Autschbach, J. Magnetic Circular Dichroism of UCl⁶⁻ in the Ligand-to-Metal Charge-Transfer Spectral Region. *Phys. Chem. Chem. Phys.* 2017, 19, 17300–17313.
- (13) Heit, Y. N.; Sergentu, D.-C.; Autschbach, J. Magnetic Circular Dichroism Spectra of Transition Metal Complexes Calculated from Restricted Active Space Wavefunctions. *Phys. Chem. Chem. Phys.* 2019, 21, 5586–5597.
- (14) Coriani, S.; Hättig, C.; Jørgensen, P.; Helgaker, T. Gauge-Origin Independent Magneto-Optical Activity within Coupled Cluster Response Theory. *J. Chem. Phys.* **2000**, *113*, 3561–3572.
- (15) Kjærgaard, T.; Jansík, B.; Jørgensen, P.; Coriani, S.; Michl, J. Gauge-Origin-Independent Coupled Cluster Singles and Doubles Calculation of Magnetic Circular Dichroism of Azabenzenes and Phosphabenzene Using London Orbitals. J. Phys. Chem. A 2007, 111, 11278–11286.
- (16) Krykunov, M.; Banerjee, A.; Ziegler, T.; Autschbach, J. Calculation of Verdet Constants with Time-Dependent Density Functional Theory: Implementation and Results for Small Molecules. J. Chem. Phys. 2005, 122, 074105.
- (17) Kjærgaard, T.; Jørgensen, P.; Thorvaldsen, A. J.; Sałek, P.; Coriani, S. Gauge-Origin Independent Formulation and Implementation of Magneto-Optical Activity within

- Atomic-Orbital-Density Based Hartree- Fock and Kohn- Sham Response Theories. *J. Chem. Theory Comput.* **2009**, *5*, 1997–2020.
- (18) Sun, S.; Williams-Young, D.; Li, X. An Ab Initio Linear Response Method for Computing Magnetic Circular Dichroism Spectra with Nonperturbative Treatment of Magnetic Field. J. Chem. Theory Comput. 2019, 15, 3162–3169, PMID: 30933558.
- (19) Goings, J. J.; Lestrange, P. J.; Li, X. Real-Time Time-Dependent Electronic Structure Theory. WIREs Computational Molecular Science 2018, 8, e1341.
- (20) Yabana, K.; Bertsch, G. F. Application of the Time-Dependent Local Density Approximation to Optical Activity. *Phys. Rev. A* **1999**, *60*, 1271–1279.
- (21) Goings, J. J.; Li, X. An Atomic Orbital Based Real-Time Time-Dependent Density Functional Theory for Computing Electronic Circular Dichroism Band Spectra. J. Chem. Phys. 2016, 144, 234102.
- (22) Lee, K.-M.; Yabana, K.; Bertsch, G. Magnetic Circular Dichroism in Real-Time Time-Fependent Density Functional Theory. *J. Chem. Phys.* **2011**, *134*, 144106.
- (23) Vignale, G.; Rasolt, M. Density-Functional Theory in Strong Magnetic Fields. *Phys. Rev. Lett.* **1987**, *59*, 2360–2363.
- (24) Vignale, G.; Rasolt, M. Density-Functional Theory in Strong Magnetic Fields. *Phys. Rev. Lett.* **1989**, *62*, 115–115.
- (25) Vignale, G.; Rasolt, M. Current- and Spin-Density-Functional Theory for Inhomogeneous Electronic Systems in Strong Magnetic Fields. Phys. Rev. B 1988, 37, 10685–10696.
- (26) Vignale, G.; Rasolt, M. Erratum: Current- and Spin-Density-Functional Theory for Inhomogeneous Electronic Systems in Strong Magnetic Fields. Phys. Rev. B 1989, 39, 5475–5475.

- (27) Capelle, K.; Vignale, G. Nonuniqueness and Derivative Discontinuities in Density-Functional Theories for Current-Carrying and Superconducting systems. *Phys. Rev.* B **2002**, *65*, 113106.
- (28) Tellgren, E. I.; Teale, A. M.; Furness, J. W.; Lange, K.; Ekström, U.; Helgaker, T. Non-Perturbative Calculation of Molecular Magnetic Properties within Current-Density Functional Theory. J. Chem. Phys. 2014, 140, 034101.
- (29) Reimann, S.; Borgoo, A.; Austad, J.; Tellgren, E. I.; Teale, A. M.; Helgaker, T.; Stop-kowicz, S. Kohn–Sham Energy Decomposition for Molecules in a Magnetic Field. Mol. Phys. 2019, 117, 97–109.
- (30) Reimann, S.; Borgoo, A.; Tellgren, E. I.; Teale, A. M.; Helgaker, T. Magnetic-Field Density-Functional Theory (BDFT): Lessons from the Adiabatic Connection. J. Chem. Theory Comput. 2017, 13, 4089–4100, PMID: 28768100.
- (31) Grayce, C. J.; Harris, R. A. Magnetic-Field Density-Functional Theory. *Phys. Rev. A* **1994**, *50*, 3089–3095.
- (32) London, F. Théorie quantique des courants interatomiques dans les combinaisons aromatiques. J. phys. radium 1937, 8, 397–409.
- (33) Ditchfield, R. Molecular Orbital Theory of Magnetic Shielding and Magnetic Susceptibility. J. Chem. Phys. 1972, 56, 5688–5691.
- (34) Wolinski, K.; Hinton, J. F.; Pulay, P. Efficient Implementation of the Gauge-Independent Atomic Orbital Method for NMR Chemical Shift Calculations. J. Am. Chem. Soc. 1990, 112, 8251–8260.
- (35) Bouten, R.; Baerends, E.; Van Lenthe, E.; Visscher, L.; Schreckenbach, G.; Ziegler, T. Relativistic Effects for NMR Shielding Constants in Transition Metal Oxides Using the Zeroth-Order Regular Approximation. J. Phys. Chem. A 2000, 104, 5600-5611.

- (36) Krykunov, M.; Autschbach, J. Calculation of Origin-Independent Optical Rotation Tensor Components in Approximate Time-Dependent Density Functional Theory. J. Chem. Phys. 2006, 125, 034102.
- (37) Autschbach, J. Analyzing NMR Shielding Tensors Calculated with Two-Component Relativistic Methods Using Spin-Free Localized Molecular Orbitals. *J. Chem. Phys.* **2008**, *128*, 164112.
- (38) Helgaker, T.; Jaszuński, M.; Ruud, K. Ab initio Methods for the Calculation of NMR Shielding and Indirect Spin-Spin Coupling Constants. *Chem. Rev.* **1999**, *99*, 293–352.
- (39) Helgaker, T.; Coriani, S.; Jørgensen, P.; Kristensen, K.; Olsen, J.; Ruud, K. Recent Advances in Wave Function-Based Methods of Molecular-Property Calculations. *Chem. Rev.* 2012, 112, 543–631.
- (40) Sun, S.; Williams-Young, D.; Stetina, T. F.; Li, X. Generalized Hartree-Fock with Non-perturbative Treatment of Strong Magnetic Field: Application to Molecular Spin Phase Transition. J. Chem. Theory Comput. 2019, 15, 348–356.
- (41) Helgaker, T.; Taylor, P. R. In *Modern Electronic Structure Theory*; Yarkony, D. R., Ed.; World Scientific Publishing Co. Pte. Ltd.: Singapore, 1995; Chapter 12, pp 725–856.
- (42) Ding, F.; Liang, W.; Chapman, C. T.; Isborn, C. M.; Li, X. On the Gauge Invariance of Nonperturbative Electronic Dynamics Using the Time-Dependent Hartree-Fock and Time-Dependent Kohn-Sham. J. Chem. Phys. **2011**, 135, 164101.
- (43) Lestrange, P. J.; Egidi, F.; Li, X. The Consequences of Improperly Describing Oscillator Strengths Beyond the Electric Dipole Approximation. J. Chem. Phys. 2015, 143, 234103.
- (44) Epstein, S. T. Gauge Invariance of the Hartree-Fock Approximation. *J. Chem. Phys.* **1965**, *42*, 2897–2898.

- (45) Epstein, S. Gauge Invariance, Current Conservation, and GIAO's. *J. Chem. Phys.* **1973**, 58, 1592–1595.
- (46) Gauss, J.; Stanton, J. F. Electron-Correlated Approaches for the Calculation of NMR Chemical Shifts. *Adv. Chem. Phys.* **2002**, *123*, 355–422.
- (47) Schindler, M.; Kutzelnigg, W. Theory of Magnetic Susceptibilities and NMR Chemical Shifts in Terms of Localized Quantities. II. Application to Some Simple Molecules. J. Chem. Phys. 1982, 76, 1919–1933.
- (48) Kutzelnigg, W. Theory of Magnetic Susceptibilities and NMR Chemical Shifts in Terms of Localized Quantities. *Israel J. Chem.* **1980**, *19*, 193–200.
- (49) Piepho, S. B.; Schatz, P. N. Group Theory in Spectroscopy: with Applications to Magnetic Circular Dichroism; Wiley-Interscience, 1983; Vol. 1.
- (50) Economou, E. N. Green's Functions in Quantum Physics; Springer, 2006.
- (51) Oddershede, J.; Jørgensen, P.; Yeager, D. L. Polarization Propagator Methods in Atomic and Molecular Calculations. *Comput. Phys. Rep.* **1984**, *2*, 33 92.
- (52) Olsen, J.; Jørgensen, P. Linear and Nonlinear Response Functions for an Exact State and for an MCSCF State. *J. Chem. Phys.* **1985**, *82*, 3235–3264.
- (53) Petrone, A.; Williams-Young, D. B.; Sun, S.; Stetina, T. F.; Li, X. An Efficient Implementation of Two-Component Relativistic Density Functional Theory with Torque-Free Auxiliary Variables. *Euro. Phys. J. B* **2018**, *91*, 169.
- (54) Egidi, F.; Sun, S.; Goings, J. J.; Scalmani, G.; Frisch, M. J.; Li, X. Two-Component Non-Collinear Time-Dependent Spin Density Functional Theory for Excited State Calculations. J. Chem. Theory Comput. 2017, 13, 2591–2603.
- (55) Becke, A. D. A Multicenter Numerical Integration Scheme for Polyatomic Molecules. J. Chem. Phys. 1988, 88, 2547–2553.

- (56) Stratmann, R.; Scuseria, G. E.; Frisch, M. J. Achieving Linear Scaling in Exchange-Correlation Density Functional Quadratures. *Chem. Phys. Lett.* **1996**, *257*, 213 223.
- (57) Li, X.; Smith, S. M.; Markevitch, A. N.; Romanov, D. A.; Levis, R. J.; Schlegel, H. B. A Time-Dependent Hartree-Fock Approach for Studying the Electronic Optical Response of Molecules in Intense Fields. *Phys. Chem. Chem. Phys.* 2005, 7, 233–239.
- (58) Li, X.; Tully, J. C.; Schlegel, H. B.; Frisch, M. J. Ab Initio Ehrenfest Dynamics. *J. Chem. Phys.* **2005**, *123*, 084106.
- (59) Isborn, C. M.; Li, X.; Tully, J. C. TDDFT Ehrenfest Dynamics: Collisions between Atomic Oxygen and Graphite Clusters. *J. Chem. Phys.* **2007**, *126*, 134307.
- (60) Liang, W.; Chapman, C. T.; Li, X. Efficient First-Principles Electronic Dynamics. *J. Chem. Phys.* **2011**, *134*, 184102.
- (61) Li, X.; Frisch, M. J. Energy-Represented Direct Inversion in the Iterative Subspace within a Hybrid Geometry Optimization Method. *J. Chem. Theory Comput.* **2006**, *2*, 835–839.
- (62) Frisch, M. J.; Trucks, G. W.; Schlegel, H. B.; Scuseria, G. E.; Robb, M. A.; Cheeseman, J. R.; Scalmani, G.; Barone, V.; Petersson, G. A.; Nakatsuji, H.; Li, X.; Caricato, M.; Marenich, A. V.; Bloino, J.; Janesko, B. G.; Gomperts, R.; Mennucci, B.; Hratchian, H. P.; Ortiz, J. V.; Izmaylov, A. F.; Sonnenberg, J. L.; Williams-Young, D.; Ding, F.; Lipparini, F.; Egidi, F.; Goings, J.; Peng, B.; Petrone, A.; Henderson, T.; Ranasinghe, D.; Zakrzewski, V. G.; Gao, J.; Rega, N.; Zheng, G.; Liang, W.; Hada, M.; Ehara, M.; Toyota, K.; Fukuda, R.; Hasegawa, J.; Ishida, M.; Nakajima, T.; Honda, Y.; Kitao, O.; Nakai, H.; Vreven, T.; Throssell, K.; Montgomery, J. A., Jr.; Peralta, J. E.; Ogliaro, F.; Bearpark, M. J.; Heyd, J. J.; Brothers, E. N.; Kudin, K. N.; Staroverov, V. N.; Keith, T. A.; Kobayashi, R.; Normand, J.; Raghavachari, K.; Rendell, A. P.; Burant, J. C.; Iyengar, S. S.; Tomasi, J.; Cossi, M.; Millam, J. M.; Klene, M.;

- Adamo, C.; Cammi, R.; Ochterski, J. W.; Martin, R. L.; Morokuma, K.; Farkas, O.; Foresman, J. B.; Fox, D. J. Gaussian 16 Revision B.01. 2016; Gaussian Inc. Wallingford CT.
- (63) Becke, A. D. Density-Functional Thermochemistry. III. The Role of Exact Exchange.
 J. Chem. Phys. 1993, 98, 5648.
- (64) Lee, C.; Yang, W.; Parr, R. G. Development of the Colle-Salvetti Correlation-Energy Formula into a Functional of the Electron Density. *Phys. Rev. B* **1988**, *37*, 785.
- (65) Miehlich, B.; Savin, A.; Stoll, H.; Preuss, H. Results Obtained with the Correlation Energy Density Functionals of Becke and Lee, Yang and Parr. Chem. Phys. Lett. 1989, 157, 200–206.
- (66) Hariharan, P. C.; Pople, J. A. The Influence of Polarization Functions on Molecular Orbital Hydrogenation Energies. *Theor. Chem. Acc.* **1973**, *28*, 213–222.
- (67) Francl, M. M.; Pietro, W. J.; Hehre, W. J.; Binkley, J. S.; Gordon, M. S.; DeFrees, D. J.; Pople, J. A. Self-consistent molecular orbital methods. XXIII. A polarization-type basis set for second-row elements. *J. Chem. Phys.* **1982**, *77*, 3654–3665.
- (68) Williams-Young, D. B.; Petrone, A.; Sun, S.; Stetina, T. F.; Lestrange, P.; Hoyer, C. E.; Nascimento, D. R.; Koulias, L.; Wildman, A.; Kasper, J.; Goings, J. J.; Ding, F.; DePrince III, A. E.; Valeev, E. F.; Li, X. The Chronus Quantum (ChronusQ) Software Package. arXiv Preprint 2019,
- (69) Kaito, A.; Hatano, M.; Tajiri, A. CNDO Treatment for Faraday B Terms of Some Azaheterocycles. J. Am. Chem. Soc. 1977, 99, 5241–5246.
- (70) Castellan, A.; Michl, J. Magnetic Circular Dichroism of Cyclic .pi.-Electron Systems.
 4. Aza Analogs of Benzene. J. Am. Chem. Soc. 1978, 100, 6824–6827.

- (71) Meier, A. A.; Wagnière, G. H. The Long-Wavelength MCD of Some Quinones and its Interpretation by Semi-empirical MO Methods. *Chem. Phys.* **1987**, *113*, 287–307.
- (72) Millefiori, S.; Gulino, A.; Casarin, M. UV Photoelectron Spectra, Reduction Potentials and MO Calculations of Intramolecularly Hydrogen-Bonded Naphtoquinones. J. Chim. Phys. 1990, 87, 317–330.

Graphical TOC Entry

